JCTC Journal of Chemical Theory and Computation

Article

pubs.acs.org/JCTC

Theoretical Study on the UVR8 Photoreceptor: Sensing Ultraviolet-B by Tryptophan and Dissociation of Homodimer

Xin Li,*[,†] Lung Wa Chung,[§,‡] Keiji Morokuma,*[,‡] and Guohui Li*[,†]

[†]State Key Lab of Molecular Reaction Dynamics, Dalian Institute of Chemical Physics, Dalian 116023, China

[‡]Fukui Institute for Fundamental Chemistry, Kyoto University, Kyoto 606-8103, Japan

[§]Department of Chemistry, South University of Science and Technology of China, Shenzhen 518055, China

Supporting Information

ABSTRACT: By the irradiation of ultraviolet-B (UV-B) light, UVR8 photoreceptor can undergo dissociation of the protein homodimer and regulate gene expression in plants. We have carried out high-level quantum mechanics (QM) and ONIOM-(QM:MM) calculations and molecular dynamics (MD) simulations to study spectra of key tryptophan residues in UVR8 homodimer and to clarify the key role of important charged residues and their salt bridges as well as the feasible dissociation mechanism. First, benchmark calculations on the absorption and emission of 3-methylindole in the gas phase have been performed by different QM methods (TD-DFT, CASSCF, MS-CASPT2, and SAC-CI). Twenty different DFT functionals, including double hybrid and Minnesota functionals, were tested, but all these functionals failed to give satisfactory description of two key transitions. In comparison, SAC-CI and CASPT2 methods can give reliable transition energies and a correct order of ^1L_a and ^1L_b excited states. Furthermore, the vertical absorption and emission energies of tryptophan in UVR8 have been investigated by the ONIOM method. The present results suggest that W285 is the major chromophore of UVR8, while W233 can also sense the UV-B light and may be responsible for exciton coupling. Geometrical effects as well as electrostatic and polarization interactions with the protein matrix were found to influence optical properties of these tryptophan residues in UVR8. At the homodimeric interface, R286-D107 and R338-D44 salt bridges are suggested to play a crucial role for the UVR8 monomerization. In addition, the UV-B induced dissociation mechanism of the UVR8 homodimer has been proposed. The electrostatic repulsion between the partially negatively charged benzene ring of W285 in the ^1L_a excited state and the negatively charged D44/D107, along with electron and/or proton transfers among W285, R286 (or R338), W233 and D129, was suggested to result in the breakage of the key salt bridges, and destabilization as well as dissociation of the UVR8 dimer. The proposed mechanism also accounts for the fluorescence quenching in UVR8, and the stability and the enhanced red-shifted fluorescence in the W285F mutant.

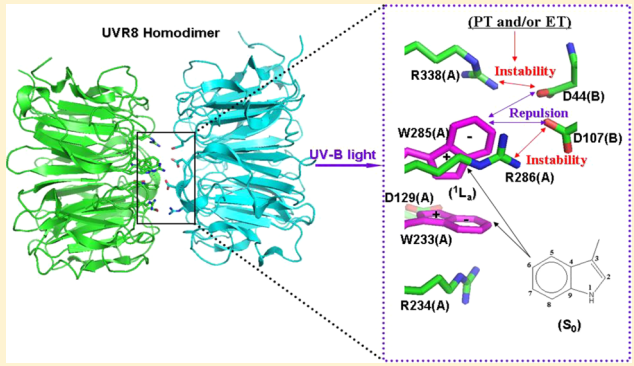

1. INTRODUCTION

Tryptophan is one of the ultraviolet (UV)-light absorbing amino acids in proteins, and its behavior is quite sensitive to the different protein environments.[1] Optical properties of tryptophan in proteins are very important for investigating complex biological processes, because absorption and emission of tryptophan including two lowest-lying states, ^1L_a and ^1L_b,[2,3] are dependent on environmental conditions. Therefore, understanding of the spectral tuning of tryptophan in different environments is very much crucial for chromophore development.

The UV-B light photoreceptor in UVR8 triggers dissociation of the protein homodimer into monomers and causes change in gene expression.[4−10] Recently, X-ray crystal structures of UVR8 homodimer have been obtained.[7,8] Several tryptophan residues were found at the UVR8 homodimer interface. Based on experimental studies, W285 and W233 were proposed to be important chromophores for sensing UV-B light, and W285, but not W233, was proposed to be vital for the UVR8 function.[7−9] In addition, some arginine residues (especially R286 and R338) reside near the surface, forming salt bridges to stabilize the dimer interface. Upon the irradiation of UV-B light, destabilization and destruction of the salt bridges were suggested to occur and lead to the dissociation of the homodimer.[7,8] Recently, Zhong and co-workers have reported the UV light-induced quenching dynamics in UVR8.[11]

As to theoretical studies,[12] for example, Eriksson and co-workers have investigated the UVR8 protein by homology modeling and time-dependent density functional theory (TD-DFT). They also studied molecular mechanism of UVR8 monomerization and the stability of the wide-type UVR8 dimer as well as some mutants by classical molecular dynamics (MD) simulations. As will be discussed later, however, TD-DFT

Received: April 18, 2014
Published: June 9, 2014

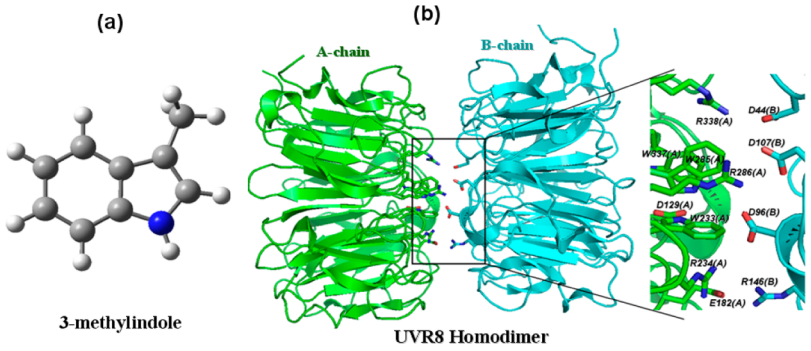

Figure 1. (a) Structure of 3-methylindole molecule and (b) the UVR8 homodimer. The positions of several key residues are highlighted by stick model.

method cannot give reliable spectroscopic properties of tryptophan. More detailed, reliable and extensive investigations on the UVR8 homodimer and its key mutants need to be performed.

In order to study spectroscopic properties of tryptophan, its indole chromophore was extensively used and investigated in experimental[13−23,24a] and theoretical studies.[24b,25−33] In general, the ^1L_b state is lower in energy than the ^1L_a state for indole in the gas phase as well as in apolar solvents, and an inversion of the order of these states occur in polar solvents.[18,21−23] It turned out that an accurate theoretical description of these two lowest-lying $\pi \rightarrow \pi^*$ transitions in indole is not trivial. Complete active space self-consistent field (CASSCF) and complete active space second-order perturbation theory (CASPT2) methods were successfully used to study spectra of indole. In contrast, popular and efficient TD-DFT methods cannot provide a good description of the two lowest-lying ^1L_a and ^1L_b excited states. In addition, TD-DFT gives a wrong order of these states and/or a wrong energy difference between the ^1L_a and ^1L_b excited states.[33,34] In addition to spectroscopic properties, excited-state deactivation channels of tryptophan were also investigated computationally by the CASPT2//CASSCF method.[35−37] On the other hand, hybrid quantum mechanics/molecular mechanics (QM/MM) methods are very powerful tools to investigate environmental effects of complex systems.[31,32,38−40]

In the present work, high-level *ab initio* quantum mechanics (QM) methods, ONIOM(QM:MM) calculations as well as molecular dynamics (MD) simulations have been carried out to reveal spectroscopic properties of UV-B chromophores in UVR8, the role of the protein environment (particularly of the key charged residues), the stability of the key salt bridges, and the possible mechanisms of the UVR8 dimer dissociation. Several QM methods, such as TD-DFT with various hybrid and double-hybrid functionals, CASSCF, MS-CASPT2, as well as SAC-CI, have been employed for benchmark calculations of absorption and emission spectra of tryptophan chromophore. Based on the benchmark results, more reliable methods are chosen and used for accurate description of the UVR8 system.

2. COMPUTATIONAL METHODS

2.1. Protein Setup and Classical Simulations. The initial structure of the UVR8 homodimer is obtained from the Protein Data Bank (PDB code: 4DNW).[8] Hydrogen atoms were added to the protein, assigning the normal protonation states of all titratable residues at the experimental pH condition on the basis of the pK_a results estimated by H++[41] and PROPKA[42] programs. Rotational orientations of histidine, asparagine, and glutamine residues were also determined by WhatCheck[43] and visual inspection to have better hydrogen bonding or less steric repulsion. Then, the protein system with crystallographic water molecules was neutralized with sodium ions and fully solvated in a cuboid box (111 × 103 × 91 Å) of TIP3P water molecules by the AMBER Leap module.[44] Molecular mechanics (MM) minimizations followed by MD simulations have been carried out in the AMBER package with an AMBER all-atom force field and TIP3P water model.[44,45] Several mutants (R286A/R338A, R286A/R146A, R286A, R338A, R146A, D96N/D107N, R200A, R234A, and R354A) have also been investigated in this work, in which similar setups and simulations were performed. The MD simulation details are given in the Supporting Information (S.I.).

2.2. QM and ONIOM(QM:MM) Calculations. The ground-state geometry optimization of a 3-methylindole molecule (Figure 1a) in the gas phase was performed by the density functional theory (DFT)[46,47h,i] and the three-state-average (SA3) CASSCF methods.[48a,b] The excited-state geometry of the 3-methylindole molecule in the gas phase was optimized by the time-dependent density functional theory (TD-DFT), SAC-CI and CASSCF methods.[46,47h,i,48a,b,49] Vertical absorption and emission energies at the optimized ground-state and excited-state structures were then calculated, respectively, by TD-DFT with 20 different functionals (including perturbatively corrected double hybrid functionals and Minnesota functionals), SAC-CI, and MS-CASPT2-(10e,9o) (with an imaginary level shift of 0.2 au) methods,[46−50] with various basis sets, BS: 6-31+G(d,p) and BS1:6-31+ +G(d,p) for DFT, BS2: def2-TZVP with RIJCOSX for double-hybrid DFT in ORCA,[50] BS3: D95(d) for SAC-CI, and BS4:6-31G*, BS5: ANO-RCC-VDZP, and BS6: ANO-RCC-VTZP for CASPT2 and CASSCF. The Gaussian 09,[51] ORCA,[50] Molcas7[52] programs were employed for the above calculations.

The protein structures (Figure 1b), which were prepared from the classical MM minimization followed by a series of snapshots from the classical MD simulations, were further refined by ONIOM(QM:MM) geometry optimization for our calculated vertical absorption and emission.[53] Solvation water molecules 3 Å far away from the protein were deleted in the ONIOM calculations. In the ONIOM(QM:MM) calculations, the QM model part and the MM part are treated by the above-mentioned high-level QM methods and the AMBER force field, respectively.[44,45] Several QM models (**A**: W285^{qm}, **B**: W233^{qm}, **C**: W285^{qm}+R286^{qm}, **D**: W285^{qm}+R338^{qm}, **E**: W233^{qm}+R234^{qm}, **F**: W285^{qm}+W233^{qm}, and **G**: W285^{qm}+W233^{qm}+W337^{qm}) have been adopted in our ONIOM calculations, including several

dx.doi.org/10.1021/ct5003362 | J. Chem. Theory Comput. 2014, 10, 3319−3330

key tryptophan and arginine residues in the A-chain of UVR8 (Supporting Information Figure S1).

In the ONIOM optimizations, the geometries of all the residues and water molecules within about 12 Å of the seven key tryptophan residues (W94, W198, W233, W250, W285, W302, and W337) at the UVR8 homodimer interface were optimized while the rest of the system is frozen at the MM minimized structure or MD simulation structures.[54] For the ground-state geometry optimization, electronic embedding (EE) scheme was employed. For the ^1L_a excited-state geometry optimization, unfortunately EE did not converge because of switching of states, and the mechanical embedding (ME) scheme was used. We found that the EE effect on the ground-state geometry of tryptophans in UVR8 is not large; ONIOM-EE and ONIOM-ME optimizations lead to very small differences of bond distances, a maximum of ∼0.004 Å for W285 and ∼0.009 Å for W233. The ONIOM-EE scheme was used to compute all absorption and emission energies in the protein.

3. RESULTS AND DISCUSSION

3.1. Absorption and Emission of 3-Methylindole in the Gas Phase. *Ground- and Excited-State Geometries.* The optimized bond lengths of 3-methylindole in the ground state (S_0) and ^1L_a and ^1L_b excited states at various levels are shown in Figure 2. As will be discussed later in detail, the ^1L_a state is mainly a charge transfer state, while ^1L_b can be regarded as a local excited state. As expected, the bond distances have similar trends between the ground state and the ^1L_b state, while those in the ^1L_a state are very different from these. Going from the equilibrium geometry in the S_0 state to the ^1L_a state, N1−C9, C2−C3 and C7−C8 bonds are stretched, while the N1−C2, C4−C9 and C6−C7 bonds are shortened. In the ^1L_a state, a large bond distance alternation is seen throughout the molecule. On the other hand, going from S_0 to ^1L_b, stretching of bond distances, in particular in the benzene ring, for C4−C9, C5−C6, C6−C7 and C7−C8 bonds, is found to take place, reflecting the nature of local excitation of benzene ring in the ^1L_b state.

As to the optimized geometries by different methods, the ground state geometries are similar among B3LYP, M06-2X and CASSCF(10e,9o). For the ^1L_a state, CASSCF and TD-B3LYP give a similar trend with a larger bond order alternation than the trend given by SAC-CI and TD-M06-2X with a smaller bond alternation. Similarly, for the ^1L_b state, CASSCF gives a larger bond order alternation than SAC-CI.

Vertical Absorption Energies and Oscillator Strengths. The calculated vertical absorption energies of 3-methylindole at the S_0 equilibrium structure (i.e., Franck−Condon (FC) point) by different QM methods are listed in Table 1 and Supporting Information Table S1. Many pure and hybrid functionals (e.g., TD-B3LYP, TD-M06-L, TD-M06, TD-M06-HF, TD-M06-2X, TD-SOGGA11X, TD-SOGGA11, TD-M11L, TD-MN12SX, and TD-N12) as well as different double-hybrid functionals (e.g., TD-B2PLYP, TD-mPW2PLYP, TD-B2GP-PLYP, TD-B2K-PLYP, and TD-B2T-PLYP) have been first tested for description of the electronic transitions from S_0 to the ^1L_b and ^1L_a excited states. In the calculations, the $S_0 \rightarrow {}^1L_b$ excitation mainly consists of excitation from HOMO−1 to LUMO as well as from HOMO to LUMO+1, while $S_0 \rightarrow {}^1L_a$ mainly consists of excitation from HOMO to LUMO as well as from HOMO−1 to LUMO+1 (Supporting Information Figure S2). Twenty

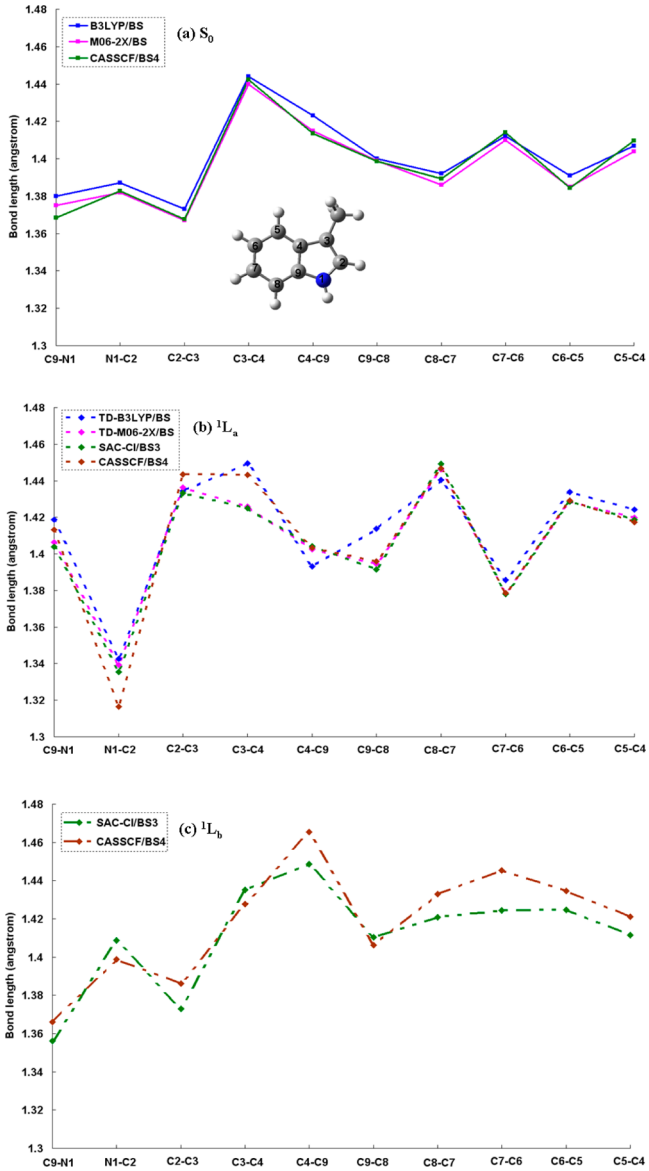

Figure 2. Optimized bond lengths of 3-methylindole in the (a) S_0, (b) ^1L_a and (c) ^1L_b states in gas phase.

different TD-DFT methods give transition energies between 4.56 and 5.17 for $S_0 \rightarrow {}^1L_b$ and 4.12−5.08 eV for $S_0 \rightarrow {}^1L_a$, which are quite deviated from the experimental values of indole (4.37 and 4.77 eV, respectively) in gas phase.[13−17] The most important fact is that all these TD-DFT methods (with one exception), including the double hybrid functionals and Minnesota functionals, give a wrong order of state for the ^1L_a and ^1L_b excited states. Therefore, as reported recently using several functionals (B3LYP, PBE0, mPW1PW91, M06-L, M06-2X, CAM-B3LYP, ωB97XD, LC-BLYP, and LC-ωPBE),[33] the TD-DFT methods with these popular or new functionals cannot give accurate absorption of the two low-lying ^1L_b and ^1L_a excited states.

The higher-level QM method used in the present test, SAC-CI method, which was shown to be very reliable to calculate absorption energies of many systems,[54a,b,55] reproduces well the vertical transition energies (and the order of the two states) for the ^1L_b and ^1L_a states ($S_0 \rightarrow {}^1L_b$: 4.37−4.42 eV and $S_0 \rightarrow {}^1L_a$: 4.81−4.84 eV, see Table 1), compared to the experimental

dx.doi.org/10.1021/ct5003362 | J. Chem. Theory Comput. 2014, 10, 3319−3330

Table 1. Computed Vertical Absorption Energies (ΔE) and Oscillator Strengths (f) of 3-Methylindole in the Gas Phase

methods	^1L_b state		^1L_a state	
	ΔE (eV)	f	ΔE (eV)	f
TD-B3LYP/BS1//B3LYP/BS	4.80	0.02	4.53	0.07
TD-M06-L/BS1//M06-2X/BS	4.79	0.02	4.45	0.06
TD-M06-2X/BS1//M06-2X/BS	5.08	0.05	4.95	0.09
TD-SOGGA11X/BS1//M06-2X/BS	5.09	0.04	4.89	0.10
TD-M11L/BS1//M06-2X/BS	4.56	0.03	4.12	0.05
TD-MN12SX/BS1//M06-2X/BS	4.93	0.01	4.62	0.05
TD-N12/BS1//M06-2X/BS	4.56	0.01	4.18	0.05
TD-B2PLYP/BS2//M06-2X/BS[a]	4.93	0.07	4.85	0.07
TD-mPW2PLYP/BS2//M06-2X/BS[a]	4.98	0.08	4.91	0.07
TD-B2GP-PLYP/BS2//M06-2X/BS[a]	5.03	0.09	4.97	0.07
TD-B2K-PLYP/BS2//M06-2X/BS[a]	5.06	0.08	5.08	0.09
TD-B2T-PLYP/BS2//M06-2X/BS[a]	5.00	0.08	4.93	0.07
SAC-CI/BS3//B3LYP/BS	4.37	0.02	4.81	0.11
SAC-CI/BS3//M06-2X/BS	4.42	0.02	4.84	0.11
SAC-CI/BS3//SA3-CASSCF/BS4	4.40	0.03	4.84	0.11
MS-CASPT2/BS4//M06-2X/BS	4.46	0.02	5.01	0.09
MS-CASPT2/BS5//M06-2X/BS	4.35	0.02	4.79	0.09
MS-CASPT2/BS6//M06-2X/BS	4.23	0.02	4.59	0.09
MS-CASPT2/BS4//SA3-CASSCF/BS4[b]	4.46	0.02	5.03	0.09
MS-CASPT2/BS5//SA3-CASSCF/BS4[b]	4.35	0.02	4.81	0.09
MS-CASPT2/BS6//SA3-CASSCF/BS4[b]	4.23	0.02	4.61	0.10
CASPT2//CASSCF[c]	4.48	0.02	4.99	0.09

[a] ^1L_a and ^1L_b states are mixed. [b] The absorption energies increase by about 0.3 eV by using IPEA of 0.2 au (see Table S3). [c] The absorption energies were calculated by CASPT2//CASSCF/6-31G* (ref 39).

values.[13−17] In addition, the $S_0 \rightarrow {}^1L_a$ transition has a larger computed oscillator strength than the $S_0 \rightarrow {}^1L_b$ transition.[56] The computed Mulliken charges of 3-methylindole (Supporting Information Figure S3) indicate that during the $S_0 \rightarrow {}^1L_a$ transition, electron is partially transferred from the pyrrole moiety to the benzene ring. On the other hand, the Mulliken charge is not changed much during the $S_0 \rightarrow {}^1L_b$ transition, confirming that ^1L_b and ^1L_a can be regarded as local-excitation and charge-transfer (CT) states, respectively.

Furthermore, the absorption energies were computed by MS-CASPT2 with different basis sets (Table 1).[57] The calculated transition energies ($S_0 \rightarrow {}^1L_b$: 4.46 eV; $S_0 \rightarrow {}^1L_a$: 5.01−5.03 eV) by the MS-CASPT2/BS4 method are also in good agreement with the previous work.[39] The MS-CASPT2/BS5 calculated absorption energies ($S_0 \rightarrow {}^1L_b$: 4.35 eV; $S_0 \rightarrow {}^1L_a$: 4.79−4.81 eV) were found to be closer to those computed by the SAC-CI/BS3 method and from the experimental data.[13−17] The MS-CASPT2 with a larger basis set (BS6) gives slightly red-shifted absorption energies ($S_0 \rightarrow {}^1L_b$: 4.23 eV; $S_0 \rightarrow {}^1L_a$: 4.59−4.61 eV). A large charge transfer (about 0.3 e) with a large dipole moment[56b] was also found in the ^1L_a excited state, supporting the charge-transfer character (see also Table S2).

Vertical Emission Energies and Oscillator Strengths. As shown in Table 2, at the ^1L_a excited-state equilibrium structures optimized by TD-DFT, SAC-CI and CASSCF, the vertical emission energy for the $^1L_a \rightarrow S_0$ transition of 3-methylindole in the gas phase was calculated. The dependency of the emission energies to the optimized geometries is rather small. The SAC-CI computed vertical emission energy is about 4.00−4.10 eV. For MS-CASPT2, increasing the basis set size from BS5 to BS6 decreases the emission energy by about 0.2 eV from 4.05−4.14 eV to 3.88−3.97 eV. These calculated results are comparable to the previous theoretical studies.[25,39]

Table 2. Computed Vertical Emission Energy for $^1L_a \rightarrow S_0$ (ΔE) and Oscillator Strength (f) of 3-Methylindole in the Gas Phase

methods	$^1L_a \rightarrow S_0$	
	ΔE (eV)	f
TD-B3LYP/BS	3.90	0.07
TD-M06-2X/BS	4.30	0.12
SAC-CI/BS3//TD-B3LYP/BS	4.09	0.13
SAC-CI/BS3//TD-M06-2X/BS	4.10	0.15
SAC-CI/BS3//SAC-CI/BS3	4.10	0.15
SAC-CI/BS3//SA3-CASSCF/BS4	4.00	0.14
MS-CASPT2/BS4//TD-B3LYP/BS	4.32	0.09
MS-CASPT2/BS5//TD-B3LYP/BS	4.12	0.09
MS-CASPT2/BS6//TD-B3LYP/BS	3.95	0.09
MS-CASPT2/BS4//TD-M06-2X/BS	4.35	0.11
MS-CASPT2/BS5//TD-M06-2X/BS	4.14	0.11
MS-CASPT2/BS6//TD-M06-2X/BS	3.96	0.11
MS-CASPT2/BS4//SAC-CI/BS3[a]	4.36	0.11
MS-CASPT2/BS5//SAC-CI/BS3	4.14	0.11
MS-CASPT2/BS6//SAC-CI/BS3	3.97	0.11
MS-CASPT2/BS4//SA3-CASSCF/BS4	4.24	0.11
MS-CASPT2/BS5//SA3-CASSCF/BS4	4.05	0.11
MS-CASPT2/BS6//SA3-CASSCF/BS4	3.88	0.11
CASPT2//CASSCF[b]	4.21	0.11

[a] ^1L_a and ^1L_b states are mixed. [b] The emission energy was calculated by CASPT2//CASSCF/6-31G* (ref 39).

At the ^1L_b excited-state equilibrium structures of 3-methylindole in the gas phase optimized by SAC-CI or CASSCF, the vertical emission energy was calculated by SAC-CI and MS-CASPT2 methods. As shown in Table 3, the SAC-CI computed emission energy is 4.08−4.14 eV, in good agreement with that calculated by the MS-CASPT2/BS4 and MS-CASPT2/BS5 methods. A somewhat lower emission energy was also obtained by the MS-CASPT2/BS6 method. The calculated emission energy of 3-methylindole in Table 3 (3.91−4.18 eV) is slightly lower than the measured value of indole in the gas phase (4.36 eV).[25]

Table 3. Computed Vertical Emission Energy (ΔE) for $^1L_b \rightarrow S_0$ and Oscillator Strength (f) of 3-Methylindole in the Gas Phase

methods	$^1L_b \rightarrow S_0$	
	ΔE (eV)	f
SAC-CI/BS3//SAC-CI/BS3	4.14	0.04
SAC-CI/BS3//SA3-CASSCF/BS4	4.08	0.03
MS-CASPT2/BS4//SAC-CI/BS3	4.18	0.03
MS-CASPT2/BS5//SAC-CI/BS3	4.07	0.03
MS-CASPT2/BS6//SAC-CI/BS3	3.95	0.03
MS-CASPT2/BS4//SA3-CASSCF/BS4	4.12	0.02
MS-CASPT2/BS5//SA3-CASSCF/BS4	4.03	0.02
MS-CASPT2/BS6//SA3-CASSCF/BS4	3.91	0.02
CASPT2//CASSCF[a]	4.12	

[a] The emission energy was calculated by CASPT2//CASSCF/6-31G*, and the oscillator strength was not reported (ref 39).

dx.doi.org/10.1021/ct5003362 | J. Chem. Theory Comput. 2014, 10, 3319−3330

Based on the above-calculated results, the high-level SAC-CI method successfully reproduces many properties, such as vertical absorption and emission energies, oscillator strengths, and dipole moments. Therefore, the SAC-CI method will be mainly used as the QM method in the subsequent ONIOM-(QM:MM) calculations for the spectra of the UVR8 homodimer. The MS-CASPT2 method was also used for comparison to study the absorption and emission energies of UVR8.

3.2. Absorption and Emission in UVR8. It has been proposed from experiments that W285 is mainly responsible for sensing the UV-B light, W233 is also important for UV-B perception (but not for function), and W337 plays a minor role.[7−9] Herein, absorption and emission energies of the key tryptophans in UVR8 were calculated by the ONIOM-(QM:MM) method with several QM models to examine the practical method for evaluating the environmental effect on the absorption and emission energies.

At the ONIOM(M06-2X/BS:AMBER)-EE optimized ground-state geometries (Supporting Information Figure S4), the largest differences of indole bond lengths among different tryptophan residues and different models are about 0.02 Å (for N1−C2, C2−C3, C4−C9 and N1−C9 bonds, Supporting Information Figure S5), and the effect of protein on structural changes of tryptophan chromophore is small.

As shown in Table 4, ONIOM(SAC-CI/BS3:AMBER)-EE calculated absorption energies (W285: 4.35 eV ($S_0 \rightarrow {}^1L_b$) and 4.66 eV ($S_0 \rightarrow {}^1L_a$); W233: 4.27 eV ($S_0 \rightarrow {}^1L_b$) and 4.10 eV ($S_0 \rightarrow {}^1L_a$)) are in good agreement with those obtained by the ONIOM(MS-CASPT2:AMBER)-EE method with a larger basis set BS5 or BS6 (W285: 4.26−4.39 eV ($S_0 \rightarrow {}^1L_b$) and 4.54−4.74 eV ($S_0 \rightarrow {}^1L_a$); W233: 4.21−4.34 eV ($S_0 \rightarrow {}^1L_b$) and 4.04−4.20 ($S_0 \rightarrow {}^1L_a$)) at the same geometries.[58] At the FC point, the ^1L_b excited state is lower than the ^1L_a excited state for W285 in UVR8 in all the different levels of the ONIOM calculations, whereas for W233 in UVR8, ^1L_b is higher than ^1L_a in the ONIOM calculations, except ONIOM(MS-CASPT2/BS4:AMBER).

Table 4. ONIOM(QM:AMBER)-EE Computed Vertical Absorption Energies (ΔE) and Oscillator Strengths (f) of Tryptophans in UVR8, Based on the ONIOM(M06-2X/BS:AMBER)-EE Optimized Geometries

	^1L_b state		^1L_a state	
QM methods	ΔE (eV)	f	ΔE (eV)	f
W285 in ONIOM model A[a]				
SAC-CI/BS3	4.35/4.32[b] (4.42)	0.03/0.03 (0.02)	4.66/4.61[b] (4.84)	0.12/0.11 (0.11)
MS-CASPT2/BS4	4.50	0.02	4.97	0.09
MS-CASPT2/BS5	4.39	0.02	4.74	0.09
MS-CASPT2/BS6	4.26 (4.23)	0.03 (0.02)	4.54 (4.59)	0.10 (0.09)
W233 in ONIOM model B[c]				
SAC-CI/BS3	4.27/4.33[b]	0.02/0.04	4.10/4.23[b]	0.07/0.06
MS-CASPT2/BS4	4.35	0.02	4.49	0.07
MS-CASPT2/BS5	4.34	0.02	4.20	0.07
MS-CASPT2/BS6	4.21	0.02	4.04	0.07

[a]In parentheses, 3-methylindole in gas phase, taken from Table 1. [b]The ONIOM-ME optimized geometry was used. [c]The ^1L_b state is mixed with the ^1L_a state.

What is the major reason for the reversal of the order of ^1L_a and ^1L_b states between W233 and W285 in the UVR8 protein? Table 4 indicates that, compared to the gas phase, the protein effect on the W285 absorption energies is not large for excitations to either ^1L_b or ^1L_a state, whereas it is larger for W233, in particular for the excitation to the ^1L_a (see also Supporting Information Tables S4−S6).[58] The ^1L_a excitation energy of W233 is lowered by as much as 0.5 eV by the protein effect. Therefore, for W233, the ^1L_a excited state is *higher* than the ^1L_b excited state by about 0.3−0.4 eV in the absence of the protein matrix (i.e., in gas phase or in the bare QM model), while the ^1L_a excited state is *lower* than the ^1L_b excited state by about 0.1−0.2 eV in the protein matrix.

Furthermore, several different ONIOM(QM:MM) models consisting of different QM parts were adopted and compared in Table 5. Models including some nearby arginine residues (R286, R338 or R234) in the QM region, models **C**-**E**, give results similar to the model **A** or **B** (Table 4) in which these residues are treated by MM. When W285 and W233 are in the QM region (model **F**) and triad tryptophans (W233, W285 and W337) are in the QM part (model **G**),[59] the computed absorption values are generally increased and become in less agreement than the small QM models. To solve this, we may need even larger QM models, which are out of reach with the SAC-CI methodology. Therefore, the small QM models A and B should be a reasonable compromise and still be suitable to study the spectra of the key tryptophan chromophores in UVR8.

Table 5. ONIOM(SAC-CI/BS3:AMBER)-EE Computed Absorption Energies (ΔE) and Oscillator Strengths (f) of Ttryptophans in UVR8, Based on the ONIOM(M06-2X/BS:AMBER)-EE Optimized Respective Geometries of Various ONIOM Models

	^1L_b state		^1L_a state	
	ΔE (eV)	f	ΔE (eV)	f
C: $W285^{qm}$+$R286^{qm}$				
W285	4.28	0.01	4.63	0.12
D: $W285^{qm}$+$R338^{qm}$				
W285	4.28	0.03	4.69	0.13
E: $W233^{qm}$+$R234^{qm}$				
W233	4.27	0.02	4.10	0.07
F: $W285^{qm}$+$W233^{qm}$				
W285	4.52	0.03	4.89	0.18
W233	4.41	0.02	4.09	0.08
G: $W285^{qm}$+$W233^{qm}$+$W337^{qm}$				
W285	4.67	0.02	4.98	0.14
W233	4.60	0.04	4.24	0.08
W337	4.64	0.06	4.78	0.13

To further assess the emission from W285 and W233 in UVR8, the vertical emission from the ^1L_a excited state (with a larger oscillator strength than the ^1L_b state) was investigated. First, the ONIOM(TD-M06-2X/BS:AMBER)-ME method was used to optimize the UVR8 structure in the ^1L_a excited state (models A and B). The geometries of W233 and W285 in the ONIOM optimized ^1L_a structures are similar to those in gas phase. As listed in Table 6, the ONIOM(SAC-CI:AMBER)-EE single point calculations give the vertical emission energy of 3.63 eV for W285 in UVR8, which agrees with 3.64 eV

dx.doi.org/10.1021/ct5003362 | J. Chem. Theory Comput. 2014, 10, 3319−3330

Table 6. ONIOM(QM:MM)-EE Computed Emission Energies (ΔE) from the ^1L_a Excited State and Oscillator Strengths (f) of Tryptophans in UVR8, Based on the ONIOM (TD-M06-2X/BS:AMBER)-ME optimized ^1L_a Excited-State Geometry

	$^1L_a \rightarrow S_0$	
QM methods	ΔE (eV)	f
W285 in ONIOM model A		
SAC-CI/BS3	3.63	0.13
MS-CASPT2/BS4	4.04	0.12
MS-CASPT2/BS5	3.84	0.12
MS-CASPT2/BS6	3.64	0.12
W233 in ONIOM model B		
SAC-CI/BS3	3.32	0.09
MS-CASPT2/BS4	3.72	0.09
MS-CASPT2/BS5	3.57	0.09
MS-CASPT2/BS6	3.44	0.09

computed by the ONIOM(MS-CASPT2/BS6:AMBER)-EE method. For W233 in UVR8, the calculated emission energies are 3.32 and 3.44 eV by the ONIOM(SAC-CI:AMBER)-EE and ONIOM(MS-CASPT2/BS6:AMBER)-EE methods, respectively. Comparison with the observed emission of 3.70 eV in the experiment[8] suggests that W285 should be the chromophore mainly responsible for the emission in UVR8. The emission energies calculated for the bare tryptophans at the ONIOM-optimized UVR8 geometries are much larger than in the protein and are closer to the gas-phase values (Table S10). Obviously, the protein largely decreases the energy difference between the ^1L_a and S_0 states of W285 and W233 (more so for W233) at the ^1L_a optimized geometries.

3.3. Effect of Charged Residues on Absorption and Emission. In order to further evaluate the effects (electrostatic and polarization effects) of individual charged residues on the spectra of UVR8, the absorption and emission energies of W285 and W233 were also calculated in the absence of the side-chain atomic charges of nearby charged residues close to the UVR8 homodimer interface (see Supporting Information Figure S4). The ONIOM (SAC-CI/BS3:AMBER)-EE method is utilized to calculate absorption and emission energies, at the ONIOM(M06-2X/BS:AMBER)-EE and -ME optimized S_0 and ^1L_a geometries, respectively. The results are shown in Figure 3 and Table 7.

First, as seen in Section 3.2, a red-shift takes place for absorption of W285 in the UVR8, compared to 3-methylindole in the gas phase. Figure 3a shows that the effect of the charged residues on the $S_0 \rightarrow {}^1L_a$ CT excitation is generally much larger than the effect on the $S_0 \rightarrow {}^1L_b$ local excitation. For instance, the absence of the charges on R338, which is near the benzene ring of W285, increases the $S_0 \rightarrow {}^1L_a$ excitation energy of W285 by about 0.2 eV, but does not change the $S_0 \rightarrow {}^1L_b$ excitation energy. R338 makes the largest contribution to the red-shifted absorption of W285 in UVR8. Comparatively, the effect of R286 and R354 on the $S_0 \rightarrow {}^1L_a$ transition is smaller. Some negatively charged residues, D96(B) (D96 in the B chain), D129 and E182, provide additional preferential stabilization to the partially positively charged pyrrole moiety of W285 in the ^1L_a excited state, with respect to the ground state. Therefore, these three residues make smaller but significant contribution to the red-shift of the absorption of W285 in UVR8. On the other hand, negatively charged D44(B) and D107(B) (D44 and D107 in the B chain) are close to the partially negatively charged benzene ring and thus destabilize the ^1L_a excited state, contributing to blue-shift or reduction of the net red-shift of the absorption energy.

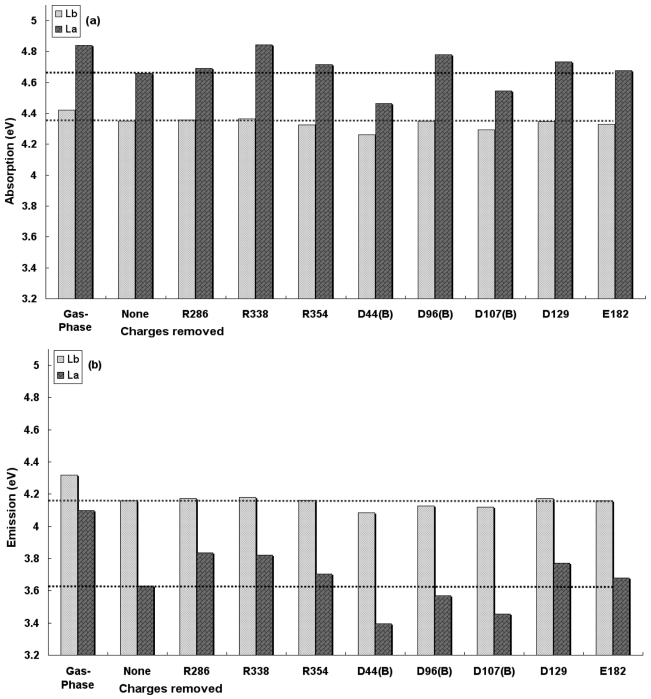

Figure 3. Effects of removing side-chain charges of key charged residues on (a) absorption and (b) emission of W285 in UVR8, compared with 3-methylindole in the gas phase. For UVR8, model A was used with the ONIOM(SAC-CI/BS3:AMBER)-EE method at the ONIOM (M06-2X/BS:AMBER)-EE ground-state and ONIOM(TD-M06-2X/BS:AMBER)-ME ^1L_a excited-state optimized geometries.

Table 7. Effects of Side-Chain Atomic Charges on the ONIOM(SAC-CI:AMBER)-EE Computed Vertical Absorption and Emission Energies (ΔE) and Oscillator Strengths (f) of W233 in UVR8, Based on the Model B ONIOM(M06-2X:AMBER) Optimized Geometries

	$S_0 \rightarrow {}^1L_b$		$S_0 \rightarrow {}^1L_a$		$^1L_a \rightarrow S_0$	
removed charges	ΔE (eV)	f	ΔE (eV)	f	ΔE (eV)	f
none	4.27	0.02	4.10	0.07	3.32	0.09
R146(B)	4.29	0.02	4.20	0.08	3.40	0.09
R234	4.26	0.02	4.45	0.10	3.74	0.13
D129	4.30	0.02	4.49	0.11	3.68	0.12
E182	4.24	0.02	4.00	0.06	3.24	0.08

Second, the effect of these charged residues on the emission of W285 is discussed. The first excited state of W285 is the ^1L_a excited state, and the charged residues largely influence this $^1L_a \rightarrow S_0$ CT transition (Figure 3b). As discussed in Section 3.2, the emission energy of W285 in UVR8 exhibited a large red shift, compared to 3-methylindole in the gas phase. Figure 3b shows that this red shift is induced mainly by R286 and R338 through large stabilization of the CT ^1L_a excited state. Comparatively, the effect of R354 on the emission energy is smaller, since it is farther away from W285. On the other hand, the negatively charged D44(B), D96(B) and D107(B) destabilize the ^1L_a excited state, resulting in a blue-shift or a reduction of the net red-shift of emission. In contrast, D129 and E182 contribute to a red-shift in emission of W285 in UVR8.

dx.doi.org/10.1021/ct5003362 | J. Chem. Theory Comput. 2014, 10, 3319−3330

The above-mentioned electrostatic and polarization effects of the charged residues on the absorption and emission energies of W285 in the UVR8 protein can be supported by the charge distribution of W285 in S_0, ^1L_a and ^1L_b states (Supporting Information Figure S9). There is evidently a nice correlation between the absorption/emission in Figure 3 and the corresponding charge distribution in Supporting Information Figure S9. For instance, the enhancement of charge transfer in the ^1L_a excited state of W285 is found when one eliminates the side-chain atomic charges of D44(B) or D107(B). In contrast, the charge translocation is reduced in the absence of the side-chain charges of R338. For the $^1L_a \rightarrow S_0$ transition, a decreased charge transfer in the ^1L_a excited state of W285 is caused by removal of the side-chain charges of R286. These illustrate that some key charged residues have significant effects in the spectra of W285 in UVR8.

Finally, as shown in Table 7, R234 and D129 were found to have the largest effect on the absorption and emission energies of W233 in the protein, controlling its optical property. The two residues stabilize the CT ^1L_a excited state so much that the $S_0 \rightarrow {}^1L_a$ transition becomes lower in energy than the $S_0 \rightarrow {}^1L_b$ transition, and its $^1L_a \rightarrow S_0$ emission energy smaller than that of W285 in UVR8. When the side-chain atomic charges of R234 or D129 are removed, the absorption and emission energies of W233 become similar to those of W285 in UVR8. In addition, R146(B) (R146 in the B chain) and E182, a little far away from W233, also stabilizes and destabilizes the ^1L_a excited state of W233, respectively, and thus red-shift and blue-shift the transition energies, respectively. The charge analysis of W233 in S_0, ^1L_a, and ^1L_b states (Supporting Information Table S11) shows that, when the side-chain charges of R234 or D129 are removed, the charges on the pyrrole and benzene rings of W233 become "normal", similar to the charge distribution of the isolated tryptophan model.

All in all, the charges and relative position/orientation of these charged residues determine the protein effects on the absorption and emission of tryptophan. Due to the charge-transfer nature of the ^1L_a excited state of tryptophan, some key charged residues interact strongly with the partially negatively charged benzene ring and/or the partially positively charged pyrrole moiety of the tryptophan chromophore. As a result, these charged residues stabilize or destabilize the CT ^1L_a excited state, and thus, tune the spectroscopic property of tryptophan in UVR8.

3.4. Effect of the Protein Conformations on Absorption and Emission. Now the effects of the protein conformations on the spectra of tryptophan will be evaluated. At first 150−180 snapshots were taken from the classical MD simulations of UVR8.[60] Then, the geometries of W285 and W233 in the S_0 and ^1L_a states were further optimized by the ONIOM(M06-2X/BS:AMBER)-EE and ONIOM (TD-M06-2X/BS:AMBER)-ME methods, respectively.[61] The vertical absorption and emission energies of W285 and W233 in the protein were computed for all these optimized geometries by the ONIOM(SAC-CI:AMBER)-EE method.

Table 8 and Figure 4 show the average and distribution of absorption and emission energies of W285 and W233 in UVR8. The ^1L_b excitation energy of W285 is in the range of 4.18−4.36 eV, with an average value of 4.29 eV, while the ^1L_b excitation energy of W233 ranges from 4.19 to 4.42 eV (with an average value of 4.32 eV). Relative to the $S_0 \rightarrow {}^1L_b$ absorption, a broader $S_0 \rightarrow {}^1L_a$ absorption band was found. For the $S_0 \rightarrow {}^1L_a$ transition, the absorption of W285 ranges from 4.19 to 4.76 eV (with an average value of 4.48 eV), and the absorption of W233 is in the range of 4.11−4.69 eV (with an average value of 4.43 eV). Therefore, there is more overlap of the absorption bands between the $S_0 \rightarrow {}^1L_b$ and $S_0 \rightarrow {}^1L_a$ transitions of W233, compared to that of W285. As found by comparing Tables 4 and 8, the conformational averaging of the protein structure leads to a red-shifted absorption of W285 and a blue-shifted absorption of W233 in UVR8.

The emission energy of W285 is found to be similar to that of W233 in UVR8, in the range of 3.28−3.85 eV (with an average value of ∼3.6 eV). The calculated emission energy is comparable to the experimental value (3.70 eV).[8] However, based on the ONIOM-optimized protein crystal structure, the

Table 8. ONIOM(SAC-CI:AMBER)-EE Computed Average Vertical Absorption/Emission Energies (ΔE) and Oscillator Strengths (f) of W285 and W233 in UVR8 Taken from MD Snapshots with Further ONIOM Optimized Structures[a]

	$S_0 \rightarrow {}^1L_b$		$S_0 \rightarrow {}^1L_a$		$^1L_a \rightarrow S_0$	
	ΔE (eV)	f	ΔE (eV)	f	S_0	f
W285 in model A	4.29	0.02	4.48	0.09	3.60	0.11
$W285^{bare}$ in model A	4.29	0.03	4.66	0.11	3.89	0.14
W233 in model B	4.32	0.03	4.43	0.09	3.56	0.11
$W233^{bare}$ in model B	4.31	0.03	4.67	0.12	3.90	0.14

[a]Comparison with the "bare" chromophore is included. Note that "bare" means that the isolated QM calculation was performed for the chromophore with its geometry optimized in ONIOM model A or B of UVR8.

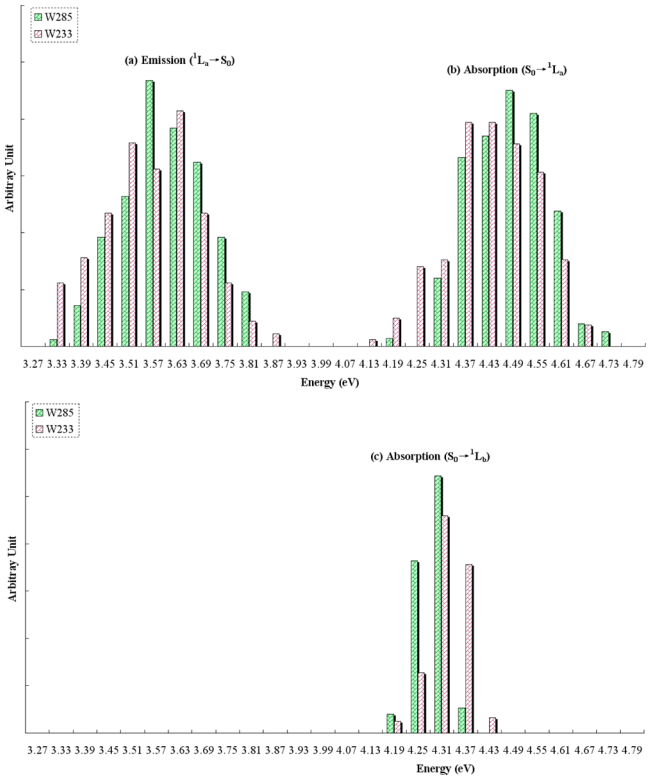

Figure 4. Histograms of distribution of the ONIOM computed (a) $^1L_a \rightarrow S_0$ emission, (b) $S_0 \rightarrow {}^1L_a$ absorption and (c) $S_0 \rightarrow {}^1L_b$ absorption for W285 and W233 in UVR8, obtained at geometries of models A and B taken from MD snapshots with the further optimization by the ONIOM method.

dx.doi.org/10.1021/ct5003362 | J. Chem. Theory Comput. 2014, 10, 3319−3330

computed emission energies of W285 and W233 were 3.63 and 3.32 eV, respectively (Table 6). The calculated emission energy of W233 in the crystal structure of UVR8 deviates from the observed result, 3.70 eV.[8] The dynamic change of the protein conformation can lead to the blue-shifted emission of W233 in UVR8 (Figure 4 and Tables 6 and 8). However, R234 and D129 stabilize the CT ^1L_a excited state of W233 in UVR8, as discussed before. Therefore, the two residues could move closer to W233 in the ^1L_a excited state, which cannot be sampled from the ground-state simulation.

In Table 8 and Figure 4 and Supporting Information Figure S14, the average absorption and emission energies of W285 and W233 in UVR8 are compared with those for the "bare" tryptophan chromophore. For the $S_0 \rightarrow {}^1L_b$ transition, the bare chromophore model has the similar absorption energy to that in the protein. For the $S_0 \rightarrow {}^1L_a$ transition, however, the bare chromophore model exhibits a large blue-shifted absorption of W285 and W233 compared to that in UVR8. A similar trend is also observed for the $^1L_a \rightarrow S_0$ emission of W285 and W233 in UVR8 and the bare tryptophan chromophore model. Interestingly, the broad band of the ^1L_a excited state of tryptophan in the protein was not found for the bare chromophore model (Supporting Information Figure S14). *Therefore, the electrostatic and polarization interactions of the chromophore with the protein are suggested to play an important role to tune the absorption and emission of tryptophan in UVR8.* In addition, the protein stabilization on the CT ^1L_a excited state of W285 or W233 can be demonstrated by the larger positive charge on the pyrrole moiety and negative charge on the benzene ring of the tryptophan chromophore in UVR8, relative to the bare chromophore model (Supporting Information Table S13).

In comparison with 3-methylindole in the gas phase, furthermore, the SAC-CI as the QM method calculated absorption and emission of tryptophan in UVR8 and those of "bare" tryptophan without the protein matrix are red-shifted (Tables 1, 2, 4, 6 and 8). Hence, the geometric change of the chromophore, which is induced by the protein (Figure 2 and Supporting Information Figures S12−S13), results in the red-shifted absorption and emission energies. As the whole, both geometrical distortion of the tryptophan chromophore by the protein and the electrostatic as well as polarization interactions of protein affect the optical properties of tryptophan in UVR8.

3.5. MD Simulations on the Mutants. At the UVR8 interface, the hydrogen bonds between the positively- and negatively charged residues can play crucial roles in maintaining stabilization of the homodimer. Generally, the double hydrogen-bonding interactions (such as R286-D107 and R146-E182 salt bridges) are stronger than the single hydrogen bonding (such as R338-D44, R286-D96, and R354-E43/E53 salt bridges). In order to investigate the effect of these salt bridges on the UVR8 dimer dissociation, classical MD simulations of several mutants (R286A/R338A, R286A/R146A, R286A, R338A, R146A, D96N/D107N, R200A, R234A, and R354A) were carried out. According to our MD simulations of wild-type UVR8, the double hydrogen-bonding R286-D107 and R146-E182 salt bridges are very strong, and the single hydrogen-bonding R338-D44 and R354-E43 salt bridges are also stable during the simulations. Since the key salt bridges are still present in the R200A, R234A and R354A mutants, they appeared to have insignificant impact on the stability of the homodimer. The simulation results are consistent in this connection, with the experiments.[7,8] As shown in Figure 5 and

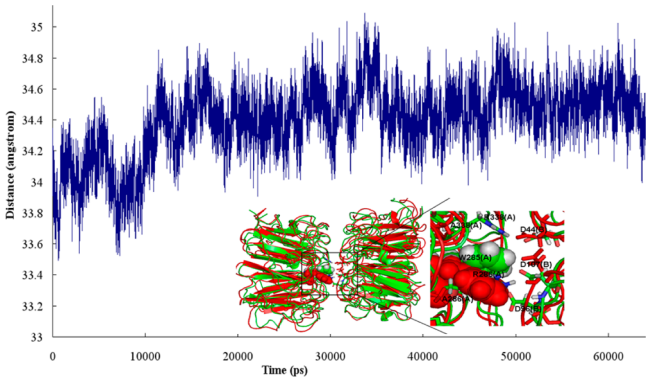

Figure 5. Distance between center of mass (COM) of monomers A and B in the MD simulation of the R286A/R338A mutant. The inserted figure is the superposition of the wide-type structure (green) and one structure after ∼60 ns MD simulation (red) of the R286A/R338A mutant.

Supporting Information Figure S15, the R286A/R338A mutant (missing the key hydrogen-bonding R286-D107/D96 and R338-D44 salt bridges) leads to the instability of the UVR8 dimer. Another mutant R286A/R146A (missing the R286-D107/D96 and R146-E182 salt bridges) also indicates a weaker interaction between monomers A and B, relative to the R146A, R286A, R338A, and D96N/D107N mutants. In our limited simulation time, the dissociation of UVR8 homodimer was not observed, which is beyond the scope of this work. In the very recent and independent work,[12a−c] Eriksson suggested that the double mutation of R286A/R338A can largely destabilize the UVR8 dimer structure.

3.6. Proposed Mechanism of UV-B Induced Dissociation of UVR8 Homodimer. The UV-B induced dissociation mechanism of the UVR8 homodimer is still under debate. Jenkins and Getzoff proposed that the electron transfer from tryptophan pyramid to its adjacent arginines in the excited state results in charge neutralization and instability of salt bridges, and then UVR8 dimer dissociates.[7] Shi and co-workers[8] suggested that the breakdown of cation−π interactions can cause the instability of salt bridges and the dissociation of the UVR8 homodimer by the UV-B irradiation of W285 and W233. Zhong recently reported a resonance energy transfer mechanism for the UV-B perception and a key role of W285 for quenching dynamics in UVR8.[11] Very recently, Eriksson proposed an electron transfer from W233 to W285 and then to R338, coupled with a proton transfer from W233 to D129 in UVR8 monomerization by the TD-DFT method, cluster approach as well as classical simulations.[12a−c] Moreover, Voityuk, Marcus and Michel-Beyerle suggested the CT "Trp285(+)-Trp233(−)" should be responsible for the breakage of salt bridges of the UVR8 dimer.[12d]

Based on the present study of the effects of protein environments on the structures and energies of ground and excited electronic states of UVR8, we propose the UV-B induced dissociation mechanism of the UVR8 homodimer, as shown in Figure 6. Upon irradiation of the UV-B light, both W285 and W233 may be excited, probably sequentially, to the ^1L_a excited state. In the ^1L_a CT excited state, R286 and R338 stabilize the partially negatively charged benzene ring of the excited W285, and R234 and D129 stabilize the benzene and pyrrole rings of W233, respectively. In addition, W233 in the CT ^1L_a excited state, bearing more negative charge on the benzene ring, interacts and stabilizes the partially positively

dx.doi.org/10.1021/ct5003362 | J. Chem. Theory Comput. 2014, 10, 3319−3330

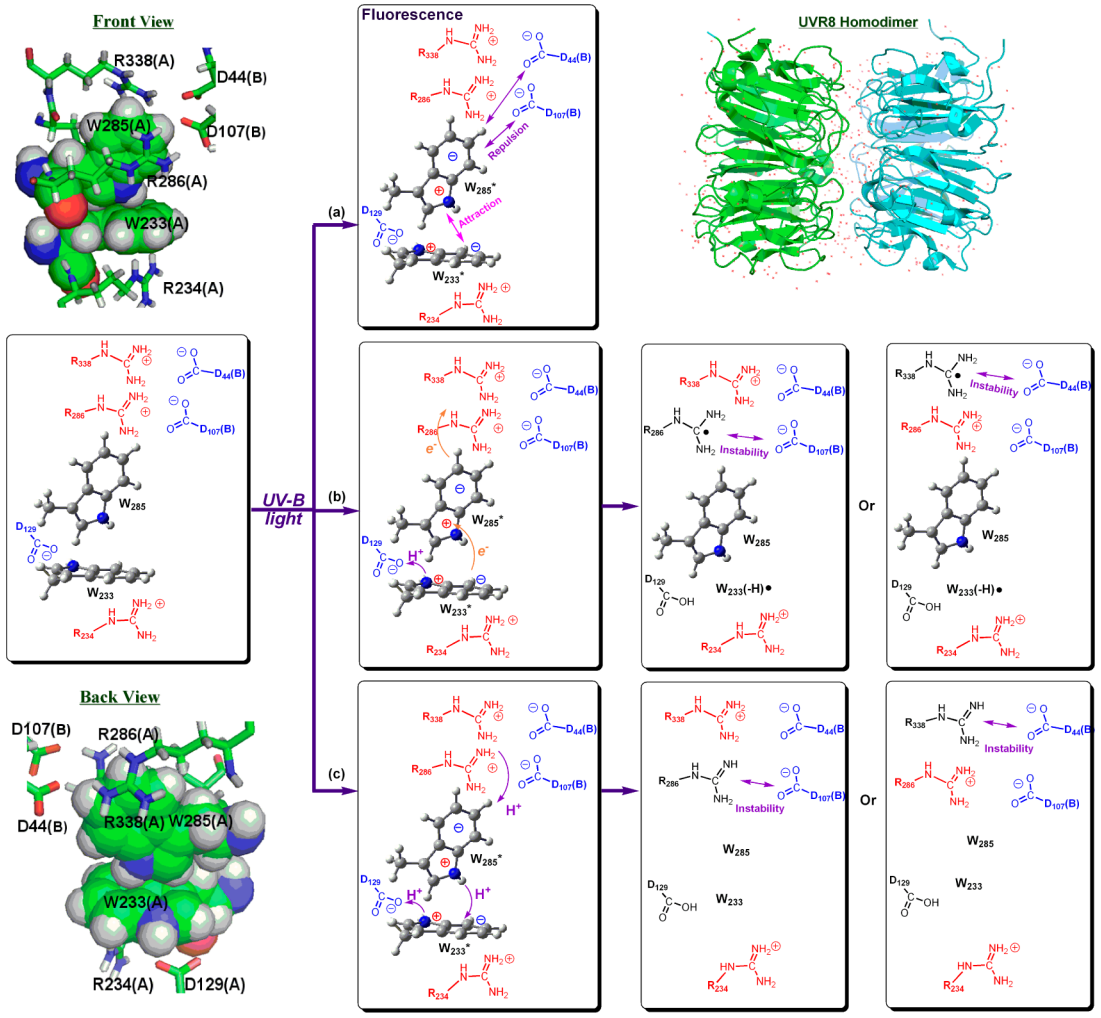

Figure 6. Proposed mechanisms of (a) fluorescence and (b) and (c), two alternative photodissociation mechanisms of the UVR8 homodimer.

charge pyrrole moiety of W285 in the ^1L_a excited state, and vice versa. In contrast, the electrostatic repulsion between W285 in the CT ^1L_a excited state and D44 and D107 in the B chain would promote the dissociation (Figure 6a).

When both W285 and W233 are excited, as shown in Figure 6b, there may be an electron transfer from the excited W285* to neutralize $R286^+$ or $R338^+$.

$$W285^* + R286^+(\text{or } R338^+) \rightarrow W285^+(\text{radical}) + R286^0 \text{ or } R338^0(\text{radical})$$

which could be coupled with another excited state electron transfer from W233* to the W285 cation radical.

$$W233^* + W285^+(\text{radical}) \rightarrow W233^+(\text{radical}) + W285$$

The produced W233 cation radical may transfer a proton to the nearby D129 anion to produce D129H neutral molecule.

$$W233^+(\text{radical}) + D129^- \rightarrow W233(-H)\text{radical} + D129H$$

The overall process is

$$W285^* + W233^* + R286^+(\text{or } R338^+) + D129^- \rightarrow W285 + W233(-H)\text{radical} + R286^0(\text{or } R338^0)\text{radical} + D129H$$

Alternatively, as shown in Figure 6c, a proton transfer may take place from $R286^+$ or $R338^+$ to W285*.

$$W285^* + R286^+(\text{or } R338^+) \rightarrow W285H^+ + R286(-H^+)^0(\text{or } R338(-H^+)^0)$$

which could be coupled with another excited state proton transfer from $W285H^+$ to W233*.

$$W233^* + W285H^+ \rightarrow W285 + W233H^+$$

The produced $W233H^+$ may transfer a proton to the nearby D129 anion to produce D129H neutral molecule.

$$W233H^+ + D129^- \rightarrow W233 + D129H$$

The overall process for this alternative is

$$W285^* + W233^* + R286^+(\text{or } R338^+) + D129^- \rightarrow W285 + W233 + R286(-H^+)^0(\text{or } R338(-H^+)^0) + D129H$$

dx.doi.org/10.1021/ct5003362 | J. Chem. Theory Comput. 2014, 10, 3319−3330

Either way, excitation energies of both W285 and W233 are used to promote this otherwise endothermic process; $R286^+$ or $R338^+$ is neutralized, and the R286-D107/D96 and/or the R338-D44 salt bridges between the two chains are weakened, and finally, the dissociation of the homodimer would take place. The reverse process for the reformation of the UVR8 homodimer could be intrinsically exothermic and may take place, probably with some activation process, in the ground electronic state.

For the W285F mutant, the non-CT nature of excited-state F285 would make the above-mentioned electrostatic repulsion, electron transfer and/or proton transfer impossible. Thus, the key salt-bridges still remain stable and the dimer would not dissociate to the monomer. Our calculations suggest that W285 and W233 are the chromophores for UV-B perception in the wild type and W233 has to be the chromophore in the W285F mutant. This explains the origin of the observed "red-shift" of fluorescence in W285F reported in the recent experiment,[11] that is, 332 nm in the wide-type UVR8 and 355 nm in the W285F mutant.

4. CONCLUSIONS

Benchmark calculations on the absorption and emission energies of 3-methylindole in the gas-phase were first carried out by various QM methods, including several DFT functionals. The 20 tested functionals, including double hybrid and Minnesota functionals, failed to give good description of the two critical electronic transitions. The spectroscopic properties of the W285 and W233 tryptophan residues in the UVR8 homodimer were then examined by the ONIOM(QM:MM) calculations. The effects of important charged residues on the optical properties of these tryptophans in the protein were also analyzed in detail. The calculations indicate that W285 is the major chromophore of UVR8, while W233 can also sense the UV-B light and may be important in the exciton coupling. Both the geometric effect (the change of tryptophan geometry in the protein) and the electronic effect (the electrostatic and polarization effect of protein on electronic structures) were found to tune the optical properties of tryptophans in UVR8. Simulations on some mutants suggest that the R286-D107 and R338-D44 salt bridges play a key role in the monomerization of the UVR8 dimer. In addition, the possible UV-B induced dissociation mechanism of the UVR8 homodimer has been proposed. In the proposed mechanism, the charge repulsion between the partially negatively charged benzene ring of W285 in the CT ^1L_a excited state and the negatively charged D44/D107 is one of the factors for the dimer dissociation. Moreover, the electron and/or proton transfer among W285, R286 or R338, W233 and D129 could result in the destruction of key salt bridges and finally lead to the dissociation of the UVR8 homodimer. Moreover, our mechanism can explain the fluorescence quenching in UVR8, and the dimer stabilization as well as the enhanced red-shifted fluorescence in the W285F mutation.

■ ASSOCIATED CONTENT

Supporting Information

Simulation details, Figures S1−S15, Tables S1−S13, and supplementary citations. This material is available free of charge via the Internet at http://pubs.acs.org.

■ AUTHOR INFORMATION

Corresponding Authors

*E-mail: lixindl@dicp.ac.cn.

*Email: morokuma.keiji.3a@kyoto-u.ac.jp.

Notes

The authors declare no competing financial interest.

■ ACKNOWLEDGMENTS

X.L. thanks DICP for the 100 Talents Support Grant. This work is partly supported by the NSFC (Grant No. 21373203) at DICP as well as JSPS Grant-in-Aid for Scientific Research <Kekenhi> No. 24245005 at Kyoto University.

■ REFERENCES

(1) Creed, D. *Photochem. Photobiol.* **1984**, *39*, 537−562.

(2) Weber, G. *Biochem. J.* **1960**, *75*, 335−345.

(3) Platt, J. R. *J. Chem. Phys.* **1949**, *17*, 484−495.

(4) Brown, B. A.; Headland, L. R.; Jenkins, G. I. *Photochem. Photobiol.* **2009**, *85*, 1147−1155.

(5) Rizzini, L.; Favory, J.-J.; Cloix, C.; Faggionato, D.; O'Hara, A.; Kaiserli, E.; Baumeister, R.; Schäfer, E.; Nagy, F.; Jenkins, G. I.; Ulm, R. *Science* **2011**, *332*, 103−106.

(6) Heijde, M.; Ulm, R. *Trends in Plant Sci.* **2012**, *17*, 230−237.

(7) Christie, J. M.; Arvai, A. S.; Baxter, K. J.; Heilmann, M.; Pratt, A. J.; O'Hara, A.; Kelly, S. M.; Hothorn, M.; Smith, B. O.; Hitomi, K.; Jenkins, G. I.; Getzoff, E. D. *Science* **2012**, *335*, 1492−1496 and references therein.

(8) Wu, D.; Hu, Q.; Yan, Z.; Chen, W.; Yan, C.; Huang, X.; Zhang, J.; Yang, P.; Deng, H.; Wang, J.; Deng, X. W.; Shi, Y. *Nature* **2012**, *484*, 214−219.

(9) O'Hara, A.; Jenkins, G. I. *Plant Cell* **2012**, *24*, 3755−3766.

(10) Cloix, C.; Kaiserli, E.; Heilmann, M.; Baxter, K. J.; Brown, B. A.; O'Hara, A.; Smith, B. O.; Christie, J. M.; Jenkins, G. I. *Proc. Natl. Acad. Sci. U. S. A.* **2012**, *109*, 16366−16370.

(11) Liu, Z.; Li, X.; Zhong, F. W.; Li, J.; Wang, L.; Shi, Y.; Zhong, D. *J. Phys, Chem. Lett.* **2014**, *5*, 69−72.

(12) (a) Wu, M.; Grahn, E.; Eriksson, L. A.; Strid, Å. *J. Chem. Inf. Model.* **2011**, *51*, 1287−1295. (b) Wu, M.; Strid, Å.; Eriksson, L. A. *J. Chem. Inf. Model.* **2013**, *53*, 1736−1746. (c) Wu, M.; Strid, Å.; Eriksson, L. A. *J. Phys. Chem. B* **2014**, *118*, 951−965. (d) During the manuscript preparation, Voityuk, Marcus and Michel-Beyerle reported the UVR8 homodimer dissociation mechanism by MS-CASPT2 calculations: Voityuk, A. A.; Marcus, R. A.; Michel-Beyerle, M.-E. *Proc. Natl. Acad. Sci. U. S. A.* **2014**, *111*, 5219−5224.

(13) Hollas, J. M. *Spectrochim. Acta* **1963**, *19*, 753−767.

(14) Lami, H. *J. Chem. Phys.* **1977**, *67*, 3274−3281.

(15) Lami, H. *Chem. Phys. Lett.* **1977**, *48*, 447−450.

(16) Bartis, T. L. O.; Grace, L. I.; Dunn, T. M.; Lubman, D. M. *J. Phys. Chem.* **1993**, *97*, 5820−5825.

(17) (a) Strickland, E. H.; Horwitz, J.; Billups, C. *Biochemistry* **1970**, *9*, 4914−4921. (b) Britten, A. Z.; Lockwood, G. *Spectrochim. Acta* **1976**, *32A*, 1335−1338.

(18) Lami, H.; Glasser, N. *J. Chem. Phys.* **1986**, *84*, 597−604.

(19) Chang, C. T.; Wu, C. Y.; Muirhead, A. R.; Lombardi, J. R. *Photochem. Photobiol.* **1974**, *19*, 347−351.

(20) Caminati, W.; Di Bernardo, S. *J. Mol. Struct.* **1990**, *240*, 253−262.

(21) Arnold, S.; Sulkes, M. *J. Phys. Chem.* **1992**, *96*, 4768−4778.

(22) Tubergen, M. J.; Levy, D. H. *J. Phys. Chem.* **1991**, *95*, 2175−2181.

(23) Short, K. W.; Callis, P. R. *J. Chem. Phys.* **2000**, *113*, 5235−5244.

(24) (a) Küpper, J.; Pratt, D. W.; Meerts, W. L.; Tatchen, J.; Schmitt, M. *Phys. Chem. Chem. Phys.* **2010**, *12*, 4980−4988. (b) Brand, C.; Küpper, J.; Pratt, D. W.; Meerts, W. L.; Krügler, D.; Tatchena, J.; Schmitt, M. *Phys. Chem. Chem. Phys.* **2010**, *12*, 4968−4979.

(25) Serrano-Andrés, L.; Roos, B. O. *J. Am. Chem. Soc.* **1996**, *118*, 185−195.

(26) Sobolewski, A. L.; Domcke, W. *Chem. Phys. Lett.* **1999**, *315*, 293−298.
(27) (a) Borin, A. C.; Serrano-Andrés, L. *Chem. Phys.* **2000**, *262*, 253−265. (b) Serrano-Andrés, L.; Borin, A. C. *Chem. Phys.* **2000**, *262*, 267−283.
(28) Sobolewski, A. L.; Domcke, W.; Dedonder-Lardeux, C.; Jouvet, C. *Phys. Chem. Chem. Phys.* **2002**, *4*, 1093−1100.
(29) Sobolewski, A. L.; Domcke, W. *J. Phys. Chem. A* **2007**, *111*, 11725−11735.
(30) Giussani, A.; Merchán, M.; Roca-Sanjuán, D.; Lindh, R. *J. Chem. Theory Comput.* **2011**, *7*, 4088−4096 and references therein.
(31) Conte, A. M.; Ippoliti, E.; Sole, R. D.; Carloni, P.; Pulci, O. *J. Chem. Theory Comput.* **2009**, *5*, 1822−1828.
(32) Wohlgemuth, M.; Bonačić-Koutecký, V.; Mitrić, R. *J. Chem. Phys.* **2011**, *135*, 054105.
(33) Arulmozhiraja, S.; Coote, M. L. *J. Chem. Theory Comput.* **2012**, *8*, 575−584 and references therein.
(34) (a) Recently, TD-DFT with double-hybrid methods (TD-B2PLYP and TD-B2GPPLYP) can correctly reproduce the state order and energy difference of two ^1L_a and ^1L_b excited states in polycyclic aromatic hydrocarbons: Goerigk, L.; Grimme, S. *J. Chem. Theory Comput.* **2011**, *7*, 3272−3277. (b) Excited state calculations and electronic energy transfer processes with TD-DFT: Jacquemin, D.; Mennucci, B.; Adamo, C. *Phys. Chem. Chem. Phys.* **2011**, *13*, 16987−16998. Caprasecca, S.; Curutchet, C.; Mennucci, B. *J. Chem. Theory Comput.* **2012**, *8*, 4462−4473. Charaf-Eddin, A.; Planchat, A.; Mennucci, B.; Adamo, C.; Jacquemin, D. *J. Chem. Theory Comput.* **2013**, *9*, 2749−2760. (c) Excited-state benchmark calculations: Schreiber, M.; Silva-Junior, M. R.; Sauer, S. P. A.; Thiel, W. *J. Chem. Phys.* **2008**, *128*, 134110. Silva-Junior, M. R.; Schreiber, M.; Sauer, S. P. A.; Thiel, W. *J. Chem. Phys.* **2008**, *129*, 104103. Sauer, S. P. A.; Schreiber, M.; Silva-Junior, M. R.; Thiel, W. *J. Chem. Theory Comput.* **2009**, *5*, 555−564.
(35) Blancafort, L.; González, D.; Olivucci, M.; Robb, M. A. *J. Am. Chem. Soc.* **2002**, *124*, 6398−6406.
(36) Grégoire, G.; Jouvet, C.; Dedonder, C.; Sobolewski, A. L. *Am. Chem. Soc.* **2007**, *129*, 6223−6231.
(37) Ovejas, V.; Fernández-Fernández, M.; Montero, R.; Castaño, F.; Longarte, A. *J. Phys. Chem. Lett.* **2013**, *4*, 1928−1932 and references therein.
(38) Rogers, D. M.; Besley, N. A.; O'Shea, P.; Hirst, J. D. *J. Phys. Chem. B* **2005**, *109*, 23061−23069.
(39) Pistolesi, S.; Sinicropi, A.; Pogni, R.; Basosi, R.; Ferré, N.; Olivucci, M. *J. Phys. Chem. B* **2009**, *113*, 16082−16090.
(40) Bernini, C.; Andrunioów, T.; Olivucci, M.; Pogni, R.; Basosi, R.; Sinicropi, A. *J. Am. Chem. Soc.* **2013**, *135*, 4822−4833.
(41) H++: http://biophysics.cs.vt.edu/H++. A server for estimating pKa's and adding missing hydrogens to macromolecules: (a) Gordon, J. C.; Myers, J. B.; Folta, T.; Shoja, V.; Heath, L. S.; Onufriev, A. *Nucleic Acids Res.* **2005**, *33*, W368−W371 (Web Server issue). (b) Bashford, D.; Karplus, M. *Biochemistry* **1990**, *29*, 10219−10225.
(42) (a) Dolinsky, T. J.; Nielsen, J. E.; McCammon, J. A.; Baker, N. A. *Nucleic Acids Res.* **2004**, *32*, W665−W667. (b) Li, H.; Robertson, A. D.; Jensen, J. H. *Proteins: Struct., Funct., Bioinf.* **2005**, *61*, 704−721.
(43) Hooft, R. W. W.; Vriend, G.; Sander, C.; Abola, E. E. *Nature* **1996**, *381*, 272.
(44) Case, D. A.; Darden, T. A.; Cheatham, III, T. E.; Simmerling, C. L.; Wang, J.; Duke, R. E.; Luo, R.; Crowley, M.; Walker, R. C.; Zhang, W.; Merz, K. M.; Wang, B.; Hayik, S.; Roitberg, A.; Seabra, G.; Kolossváry, I.; Wong, K. F.; Paesani, F.; Vanicek, J.; Wu, X.; Brozell, S. R.; Steinbrecher, T.; Gohlke, H.; Yang, L.; Tan, C.; Mongan, J.; Hornak, V.; Cui, G.; Mathews, D. H.; Seetin, M. G.; Sagui, C.; Babin, V.; Kollman, P. A. *AMBER 10*, University of California, San Francisco, 2008.
(45) (a) Cornell, W. D.; Cieplak, P.; Bayly, C. I.; Gould, I. R.; Merz, K. M., Jr.; Ferguson, D. M.; Spellmeyer, D. C.; Fox, T.; Caldwell, J. W.; Kollman, P. A. *J. Am. Chem. Soc.* **1995**, *117*, 5179−5197. (b) Jorgensen, W. L.; Chandrasekhar, J.; Madura, J. D.; Impey, R. W.; Klein, M. L. *J. Chem. Phys.* **1983**, *79*, 926−935.
(46) (a) Becke, A. D. *J. Chem. Phys.* **1993**, *98*, 5648−5652. (b) Lee, C.; Yang, W.; Parr, R. G. *Phys. Rev. B* **1988**, *37*, 785−789.
(47) (a) Peverati, R.; Truhlar, D. G. *J. Phys. Chem. Lett.* **2012**, *3*, 117−124. (b) Peverati, R.; Truhlar, D. G. *J. Chem. Theory Comput.* **2012**, *8*, 2310−2319. (c) Peverati, R.; Truhlar, D. G. *Phys. Chem. Chem. Phys.* **2012**, *14*, 13171−13174. (d) Peverati, R.; Truhlar, D. G. *Phys. Chem. Chem. Phys.* **2012**, *14*, 16187−16191. (e) Peverati, R.; Zhao, Y.; Truhlar, D. G. *J. Phys. Chem. Lett.* **2011**, *2*, 1991−1997. (f) Peverati, R.; Truhlar, D. G. *J. Chem. Phys.* **2011**, *135*, 191102. (g) Peverati, R.; Truhlar, D. G. *J. Phys. Chem. Lett.* **2011**, *2*, 2810−2817. (h) Zhao, Y.; Truhlar, D. G. *Theor. Chem. Acc.* **2008**, *120*, 215−241. (i) Jacquemin, D.; Perpète, E. A.; Ciofini, I.; Adamo, C.; Valero, R.; Zhao, Y.; Truhlar, D. G. *J. Chem. Theory Comput.* **2010**, *6*, 2071−2085. (j) Zhao, Y.; Truhlar, D. G. *J. Chem. Phys.* **2006**, *125*, 194101. (k) Zhao, Y.; Truhlar, D. G. *J. Phys. Chem. A* **2006**, *110*, 5121−5129. (l) Zhao, Y.; Truhlar, D. G. *J. Phys. Chem. A* **2006**, *110*, 13126−13130. (m) Zhao, Y.; Schultz, N. E.; Truhlar, D. G. *J. Chem. Theory Comput.* **2006**, *2*, 364−382. (n) Zhao, Y.; Schultz, N. E.; Truhlar, D. G. *J. Chem. Phys.* **2005**, *123*, 194101.
(48) (a) Roos, B. O.; Taylor, P. R.; Siegbahn, P. E. M. *Chem. Phys.* **1980**, *48*, 157−173. (b) Roos, B. O. In *Advances in Chemical Physics; Ab Initio Methods in Quantum Chemistry − II*; Lawley, K. P., Eds.; John Wiley and Sons, Ltd.: Chichester, England, 1987; Chapter 69, pp 399. (c) Andersson, K.; Malmqvist, P.-Å.; Roos, B. O.; Sadlej, A. J.; Wolinski, K. *J. Phys. Chem.* **1990**, *94*, 5483−5488. (d) Andersson, K.; Malmqvist, P.-Å.; Roos, B. O. *J. Chem. Phys.* **1992**, *96*, 1218−1226. (e) Finley, J.; Malmqvist, P.-Å.; Roos, B. O.; Serrano-Andrés, L. *Chem. Phys. Lett.* **1998**, *288*, 299−306.
(49) (a) Stratmann, R. E.; Scuseria, G. E.; Frisch, M. J. *J. Chem. Phys.* **1998**, *109*, 8218−8224. (b) Bauernschmitt, R.; Ahlrichs, R. *Chem. Phys. Lett.* **1996**, *256*, 454−464. The SAC-CI calculations using singles and doubles linked excitation operators were performed: (c) Nakatsuji, H. *Chem. Phys. Lett.* **1978**, *59*, 362−364. (d) Nakatsuji, H. *Chem. Phys. Lett.* **1989**, *67*, 329−333. (e) Nakatsuji, H. *Chem. Phys. Lett.* **1989**, *67*, 334−342.
(50) (a) Neese, F. *WIREs: Comput. Mol. Sci.* **2012**, *2*, 73−78. (b) Neese, F.; Wennmohs, F.; Hansen, A.; Becker, U. *Chem. Phys.* **2009**, *356*, 98−109. (c) Grimme, S. *J. Chem. Phys.* **2006**, *124*, 034108. (d) Schwabe, T.; Grimme, S. *Phys. Chem. Chem. Phys.* **2006**, *8*, 4398−4401.
(51) Frisch, M. J.; Trucks, G. W.; Schlegel, H. B.; Scuseria, G. E.; Robb, M. A.; Cheeseman, J. R.; Scalmani, G.; Barone, V.; Mennucci, B.; Petersson, G. A.; Nakatsuji, H.; Caricato, M.; Li, X.; Hratchian, H. P.; Izmaylov, A. F.; Bloino, J.; Zheng, G.; Sonnenberg, J. L.; Hada, M.; Ehara, M.; Toyota, K.; Fukuda, R.; Hasegawa, J.; Ishida, M.; Nakajima, T.; Honda, Y.; Kitao, O.; Nakai, H.; Vreven, T.; Montgomery, Jr., J. A.; Peralta, J. E.; Ogliaro, F.; Bearpark, M.; Heyd, J. J.; Brothers, E.; Kudin, K. N.; Staroverov, V. N.; Kobayashi, R.; Normand, J.; Raghavachari, K.; Rendell, A.; Burant, J. C.; Iyengar, S. S.; Tomasi, J.; Cossi, M.; Rega, N.; Millam, J. M.; Klene, M.; Knox, J. E.; Cross, J. B.; Bakken, V.; Adamo, C.; Jaramillo, J.; Gomperts, R.; Stratmann, R. E.; Yazyev, O.; Austin, A. J.; Cammi, R.; Pomelli, C.; Ochterski, J. W.; Martin, R. L.; Morokuma, K.; Zakrzewski, V. G.; Voth, G. A.; Salvador, P.; Dannenberg, J. J.; Dapprich, S.; Daniels, A. D.; Farkas, Ö.; Foresman, J. B.; Ortiz, J. V.; Cioslowski, J.; Fox, D. J. *Gaussian 09*, Revision C.01 and D.01; Gaussian, Inc.; Wallingford CT, 2009.
(52) (a) Aquilante, F.; De Vico, L.; Ferré, N.; Ghigo, G.; Malmqvist, P.-Å.; Neogrády, P.; Pedersen, T. B.; Pitonak, M.; Reiher, M.; Roos, B. O.; Serrano-Andrés, L.; Urban, M.; Veryazov, V.; Lindh, R. *J. Comput. Chem.* **2010**, *31*, 224−247. (b) Aquilante, F.; Pedersen, T. B.; Veryazov, V.; Lindh, R. *WIREs: Comput. Mol. Sci.* **2013**, *3*, 143−149.
(53) (a) Maseras, F.; Morokuma, K. *J. Comput. Chem.* **1995**, *16*, 1170−1179. (b) Humbel, S.; Sieber, S.; Morokuma, K. *J. Chem. Phys.* **1996**, *105*, 1959−1967. (c) Matsubara, T.; Sieber, S.; Morokuma, K. *Int. J. Quantum Chem.* **1996**, *60*, 1101−1109. (d) Svensson, M.; Humbel, S.; Froese, R. D. J.; Matsubara, T.; Sieber, S.; Morokuma, K. *J. Phys. Chem.* **1996**, *100*, 19357−19363. (e) Svensson, M.; Humbel, S.; Morokuma, K. *J. Chem. Phys.* **1996**, *105*, 3654−3661. (f) Dapprich, S.; Komáromi, I.; Byun, S.; Morokuma, K.; Frisch, M. J. *THEOCHEM*

1999, *461*, 1−21. (g) Vreven, T.; Morokuma, K. *J. Comput. Chem.* **2000**, *21*, 1419−1432. (h) Vreven, T.; Frisch, M. J.; Kudin, K. N.; Schlegel, H. B.; Morokuma, K. *Mol. Phys.* **2006**, *104*, 701−714. (i) Chung, L. W.; Hirao, H.; Li, X.; Morokuma, K. *WIREs: Comput. Mol. Sci.* **2012**, *2*, 327−350.

(54) (a) Li, X.; Chung, L. W.; Mizuno, H.; Miyawaki, A.; Morokuma, K. *J. Phys. Chem. B* **2010**, *114*, 1114−1126. (b) Li, X.; Chung, L. W.; Mizuno, H.; Miyawaki, A.; Morokuma, K. *J. Phys. Chem. B* **2010**, *114*, 16666−16675. (c) Li, X.; Chung, L. W.; Mizuno, H.; Miyawaki, A.; Morokuma, K. *J. Phys. Chem. Lett.* **2010**, *1*, 3328−3333. (d) Li, X.; Chung, L. W.; Morokuma, K. *J. Chem. Theory Comput.* **2011**, *7*, 2694−2698. (e) To avoid overpolarization of the QM wave function, the Gaussian default scaling parameters for the boundaries were used: Vreven, T.; Byun, K. S.; Komáromi, I.; Dapprich, S.; Montgomery, J. A., Jr.; Morokuma, K.; Frisch, M. J. *J. Chem. Theory Comput.* **2006**, *2*, 815−826.

(55) (a) Hasegawa, J.; Fujimoto, K.; Swerts, B.; Miyahara, T.; Nakatsuji, H. *J. Comput. Chem.* **2007**, *28*, 2443−2452. (b) Das, A. K.; Hasegawa, J.; Miyahara, T.; Ehara, M.; Nakatsuji, H. *J. Comput. Chem.* **2003**, *24*, 1421−1431. (c) Ehara, M.; Hasegawa, J.; Nakatsuji, H. In *Theory and Applications of Computational Chemistry: The First 40 Years*; Dykstra, C. E., Frenking, G., Kim, K. S., Scuseria, G. E., Eds.; Elsevier: Oxford, U.K., 2005; pp 1099−1141. (d) Hasegawa, J.; Fujimoto, K.; Nakatsuji, H. In *Quantum Systems in Chemistry and Physics Progress in Theoretical Chemistry and Physics*; Nishikawa, K., Maruani, J., Brändas, E. J., Delgado-Barrio, G., Piecuch, P., Eds.; Springer: Dordrecht Heidelberg New York London, 2012; *Vol. 26*, pp 489−502. (e) Kawatsu, T.; Hasegawa, J. *Int. J. Quantum Chem.* **2013**, *113*, 563−568. (f) Hasegawa, J.; Ise, T.; Fujimoto, K. J.; Kikuchi, A.; Fukumura, E.; Miyawaki, A.; Shiro, Y. *J. Phys. Chem. B* **2010**, *114*, 2971−2979. (g) Nakatani, N.; Hasegawa, J.; Nakatsuji, H. *J. Am. Chem. Soc.* **2007**, *129*, 8756−8765. (h) Fujimoto, K.; Hayashi, S.; Hasegawa, J.; Nakatsuji, H. *J. Chem. Theory Comput.* **2007**, *3*, 605−618.

(56) (a) The SAC-CI calculated dipole moments of the S_0, ^1L_b and ^1L_a states are 2.00−2.01, 2.42−2.50 and 5.77−5.85 D (Supporting Information Table S2), respectively, which agree with the experiments (S_0: 2.1 D, ^1L_b: 2.3 D and ^1L_a: 5.4 D): refs 18−20. (b) The CASPT2//CASSCF calculated dipole moments of the S_0 and ^1L_b states are very close, but much lower than that of the ^1L_a excited-state (Supporting Information Table S2).

(57) The slightly different equilibrium structures (obtained by different QM methods) in the ground state have little influence on the absorption energies.

(58) (a) The ONIOM-EE//ONIOM-ME calculated absorptions of W233 are a little different from those computed by the ONIOM-EE//ONIOM-EE method (Table 4). (b) The calculated dipole moments are listed in Supporting Information Table S7.

(59) (a) As shown in Supporting Information Figures S2, S6-S7 and Table S12, the $S_0 \rightarrow {}^1L_b$ and $S_0 \rightarrow {}^1L_a$ transitions ($\pi \rightarrow \pi^*$ excitations) are mainly located on W233, W285 and W337. (b) The local structure of triad tryptophans in the A-chain of UVR8 is shown in Supporting Information Figure S8. (c) Based on the ONIOM(B3LYP/BS:AMBER)-EE optimized geometries, the absorptions are also calculated (Supporting Information Table S8). (d) The computed Mulliken charges of W285 in UVR8 are displayed in Supporting Information Table S9.

(60) We extracted snapshots at about 200 ps intervals, and the first structure starts from the simulation at 2 ns, where the system is about at equilibrium (Supporting Information Figure S10). Inspection of the atom-atom distances of W233-R234 and W233-D129 (Supporting Information Figure S11) reveals the distance fluctuation of W233 and R234/ D129.

(61) The largest change of bond length is ∼0.02 Å, and there is bond distance rearrangement in the ^1L_a excited state relative to the S_0 state (Supporting Information Figures S12 and S13).